Active Role of Oxide Layers on the Polarization of Plasmonic Nanostructures

Stefania D'Agostino[†,‡,*] and Fabio Della Sala[†,§]

[†]NNL, Istituto Nanoscienze, CNR, Via Arnesano, Lecce, Italy, [‡]ISUFI-Distretto Tecnologico, Via Arnesano, Lecce, Italy, and [§]Centre of Biomolecular Nanotechnologies of IIT, Via Barsanti, Lecce, Italy

ABSTRACT In this paper a theoretical study of polarization properties of a silver nanosphere touching a homogeneous silver substrate and covered by oxide layers of increasing thickness, is reported. Oxide layers are often deposited on metallic nanostructures in metal-enhanced fluorescence (MEF) or surface-enhanced raman scattering experiments to avoid nonradiative energy transfer from emitters to the metal, and to increase the nanoparticles stability against thermal processes and laser exposure. Not much has been said on the effect of the oxide on the field enhancement of such kind of plasmonic systems. This work aims at filling this gap by shedding light on the effects of the oxide coverage on the near and far field behavior: numerical simulations performed in the framework of the discrete dipole approximation show the presence of new resonances in the absorption spectra and, of major importance for MEF applications, a strong enhancement of the near field around the nanosphere.

KEYWORDS: metal-enhanced fluorescence · plasmon · near field · oxide coverage · metal nanoparticle · discrete dipole approximation · substrate · polarization

Recent developments in nanoparticle synthesis and fabrication,[1,2] innovations in the characterization procedures and measurements,[3,4] and theoretical understanding,[5] have spread out the interest of scientists in surface plasmon-based photonics or plasmonics.[6,7] The focus is to manipulate and/or to strongly enhance the electromagnetic fields by means of surface plasmons (SPs) or localized surface plasmons (LSPs).[8] In metal nanoparticles (MNPs) the properties of LSPs (number, frequency, width, *etc.*) can be tuned by changing the particle shape and size, and the environment.[8−10] Several plasmonics applications aim at increasing the Raman scattering of organic molecules (SERS, surface-enhanced raman scattering) or the fluorescence of emitters[8,11] like colloidal nanocrystals[11] or fluorophores[12] (MEF, metal-enhanced fluorescence). In the last decades SERS measurements and similar studies, done by Fleischmann *et al.*,[13] Van Duyne and Jeanmaire[14] and Albrecht and Creighton,[15] have demonstrated that Raman scattering from pyridine on a roughened silver electrode can be enhanced by at least 6 orders of magnitude. At the same time, experimental studies using metal mirror surfaces[16−20] have shown that, due to the coupling between the LSPR and the surface plasmon, an underlying metal buffer can strongly enhance the fluorescence intensities.[21] Anyway when metal substrates are used to amplify signals, such as in biology to realize plasmonic biosensors and to detect molecular-binding events[22−24] and in (opto)electronics,[11,25−27] they can present a disadvantage which must be taken into account to realize efficient devices: at short emitter-metal distances these systems can behave like an acceptor of radiation and lead to a resonant energy transfer similar to the Forster transfer[8,28] which can strongly increase the nonradiative (NR) rate of the emitter and quench the fluorescence.

To avoid NR quenching, nonadsorbing oxide layers are often used to cover the plasmonic substrate.[25,29] These passivating layers are also useful in the prevention of surface recombination in thin-film solar cells,[30] to ensure firm contact between layers,[31] and above all to successfully protect the nanoparticles from thermal deformation[32] or enhance stability against laser exposures.[33] Concerning the effects of oxide coverages on the optical behavior of the structures on which they are deposited, experiments and theoretical modeling have been limited so far to the study of SERS and others surface-enhanced spectroscopies.[32,33,35−43]

With this work, we will study how the oxide layers affect the field enhancement factor, and we will show that an oxide layer plays an important *active* role in the optical response of a plasmonic structure, since

*Address correspondence to stefania.dagostino@le.infn.it.

Received for review December 23, 2009 and accepted May 27, 2010.

Published online June 10, 2010.
10.1021/nn1007918

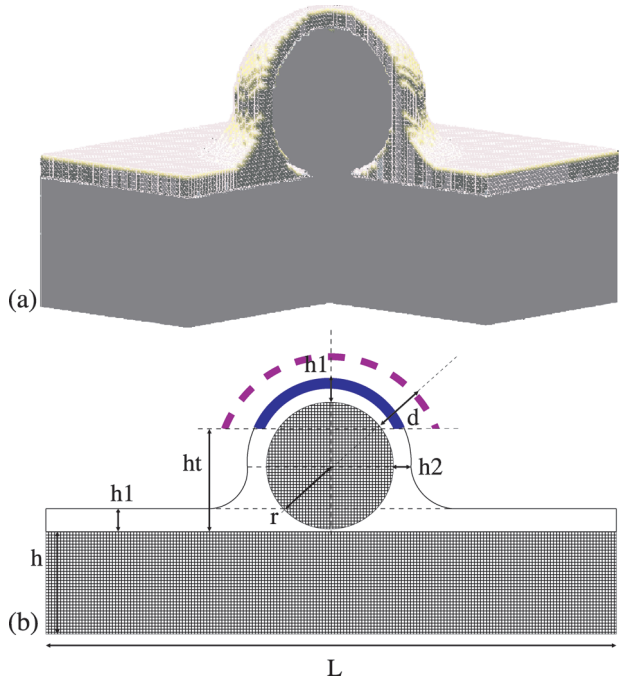

Figure 1. Schematization of the analyzed system. The pink layer in the 3D-image (a) represents the Al_2O_3 spacer covering the entire Ag structure (gray). The 2D-scheme (b) describes the geometrical parameters used to design the computational target: *h* is the height of the Ag substrate, *L* is the lateral dimension, h_1 and h_2 are, respectively, the vertical and horizontal thickness of the oxide layer, h_t is the height over which we consider the near field enhancement, *r* is the radius of the sphere, and *d* is the radial distance from the sphere surface. The dashed and solid arcs represent, respectively, examples of external and internal shells on which the field enhancement is computed.

it strongly affects the polarization of the metallic nanostructure. We consider a silver sphere deposited on a Ag buffer layer and covered by Al_2O_3 layers with different thicknesses. The optical properties of MNPs are modified by the presence of substrates,[44−47] and in particular the plasmonic substrate studied in this work and its relevance for MEF applications have recently been investigated:[29,34] for randomly distributed metal nanoparticles dispersed on a metal mirror, the coupling between the LSPRs of MNPs and the underlying metal buffer has been shown to be very useful to enhance the fluorescence of the radiators and to enlarge the fluorescence intensities.

Here the attention is focused on the perturbations induced by oxide layers on the properties of the localized SPs. In particular five important features are underlined: (i) the red-shift in the extinction spectra, (ii) the appearance of additional resonances, (iii) the strong enhancement of the near field, (iv) the nonmonotonic decay of the MEF enhancement at increasing oxide spacer, and (v) an angular redistribution of the electromagnetic field.

The results here presented could have important implications for experiments on plasmonics: as an example, the knowledge that in the presence of an oxide spacer the near field and then the MEF enhancement does not decay monotonically from the nanoparticle may lead to the consideration for SERS applications of Al_2O_3 coatings thicker than those used by Van Duyne,[39] with the possibility of providing better protection to Ag nanoparticles under the reactive environment. Moreover the nondispersive nature of an oxide makes the present study quite general: here we analyze in detail the commonly used Al_2O_3[29] but the same test-calculations done on SiO_2 revealed almost identical behavior for the two oxides (see Supporting Information).

RESULTS AND DISCUSSION

In this work, we consider a silver nanosphere with a diameter of 75 nm lying on a 70 nm-high silver substrate 500 nm large in the *y* and *z* directions (which we will refer to as S0 system) and covered by a thin layer of Al_2O_3 (5 nm, 10 nm, and 20 nm thick).

As shown in Figure 1, the oxide layers were reproduced with spheroidal concentric shells with a vertical thickness (h_1) (of 5 nm (S5), of 10 nm (S10) and of 20 nm (S20)) covering the sphere lying on the substrate. The horizontal spacers around the sphere (h_2) were taken less thick than h_1 ($h_2 = {}^4/_5 h_1$) to take into account the empirical effect of gravity. Also the entire Ag plane was covered by a h_1-thick oxide layer. The values reported in the following sections for the mean field enhancement factor ($\langle FE \rangle$) will be obtained by taking the average of the FE values calculated at each point of the external spherical shells (dashed line in panel b of Figure 1) or of the spheroidal layers internal to the oxide (solid line in panel b of Figure 1).

Being the sizes of the examined target of the same order of the wavelength of the incident light, the theoretical analysis was based on the discrete dipole approximation (DDA),[49] and calculations were performed with the ADDA code.[50]

In a recent work[29,34] we extended the ADDA code to compute the near field: we wrote an external routine,[51] able to use the polarizations found by the DDA calculations to compute the near fields outside the targets. The calculated values of the external field $\mathbf{E}_{tot}(\lambda_{exc}, \mathbf{r})$ and the **E**-field enhancements (FEs) are

$$FE(\lambda_{exc}, \mathbf{r}) = \frac{|\mathbf{E}_{tot}(\lambda_{exc}, \mathbf{r})|^2}{|\mathbf{E}_{inc}(\lambda_{exc}, \mathbf{r})|^2} = \frac{|\mathbf{E}_{inc}(\lambda_{exc}, \mathbf{r}) + \mathbf{E}_{dip}(\lambda_{exc}, \mathbf{r})|^2}{|\mathbf{E}_{inc}(\lambda_{exc}, \mathbf{r})|^2} \quad (1)$$

where $\mathbf{E}_{dip}(\lambda_{exc}, \mathbf{r})$ is the complex field at point **r** due to the superposition of the *N* dipolar fields generated by the *N* dipoles of the discretized metallic target under an excitation radiation $\mathbf{E}_{inc}(\lambda_{exc}, \mathbf{r})$ of wavelength λ_{exc} (see Methods for details).

By using an uniform incident field propagating normally to the metallic surface (along *x*) and polarized along the *y*-direction, we computed the extinction and the absorption efficiencies (see Methods) for the structures with oxide (S5, S10, and S20) and without oxide

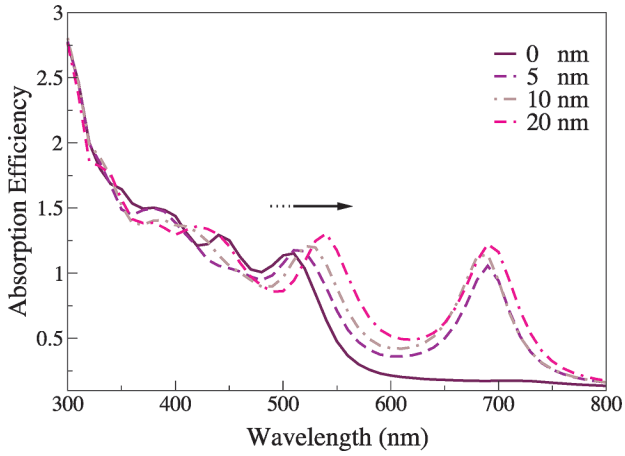

Figure 2. Comparison of the absorption spectra obtained by the DDA simulations for four different thicknesses of the Al_2O_3 layer (0, 5, 10, and 20 nm). The arrow indicates the direction of the shift of the peak-wavelengths.

(S0). The wavelengths considered in the simulations were those from 300 to 800 nm with a step of 10 nm. The obtained absorption spectra are reported in Figure 2 (for the extinction cross section see Figure S1 in the Supporting Information). Owing to the geometry of the target and the anisotropy of the space, the displacement of the electronic cloud inside the metallic structure is not homogeneous, so high-multipolar charge distributions are induced and a lot of resonant modes excited,[29] this producing the broader profile of the spectra in Figure 2.

A monotonic red-shift is clearly visible in Figure 2 by going from S0 to S20. This effect, already experimentally observed,[40] can be explained by considering the relation which lags between the dielectric function of a metallic scatterer (ε) and the dielectric constant of the surrounding background (ε_B) at the resonance condition.[44,48] According to the Quasi-static Approximation the polarizability of a particle smaller than the wavelength of the light, experiences a resonant enhancement under the conditions $Re[\varepsilon](\lambda) + ((l + 1)/l)\varepsilon_B = 0$ (with l and $l + 1$ being the exponents in the radial solutions to the Laplace's equation).[8,65] It becomes clear that by going from a few nanometers to more important spacers of Al_2O_3 the "effective" dielectric function of the confining medium increases and the frequencies of the resonant modes decrease, $Re[\varepsilon]$ of silver being a decreasing function of λ.

Moreover, by looking at the absorption spectra in Figure 2 we can see the appearance, at $\lambda_{exc} = 690$ nm, of a new resonance peak due to the oxide coverage. To understand the origin of this peak we computed for each structure at $\lambda_{exc} = 690$ nm, the absorption in the *i*-dipole position or local absorption σ_i^{abs} (see Methods). Results for S0 and S5 are reported, together to the corresponding polarization vectors-maps in Figure 3. By comparing the S0 and the S5 cases, we can observe that even if the aluminum dioxide is a "passive" (or nonabsorbing) material it produces a confinement of the electromagnetic field at the bottom side of the Ag sphere which induces a strong polarization of the metal and the excitation of the new resonance. At 690 nm, the oxide *"switches on"* the metal and a "surface-state", confined at the interface between the substrate and the particle, appears. This phenomenon is noted also through the real parts of the polarization vectors obtained for the points inside the structures (panels a and c, Figure 3). For the S0 case (a), the polarization vectors are very small and isotropically oriented; for the case of 5 nm of Al_2O_3 (c), a polarization vortex is clearly present.[52−55]

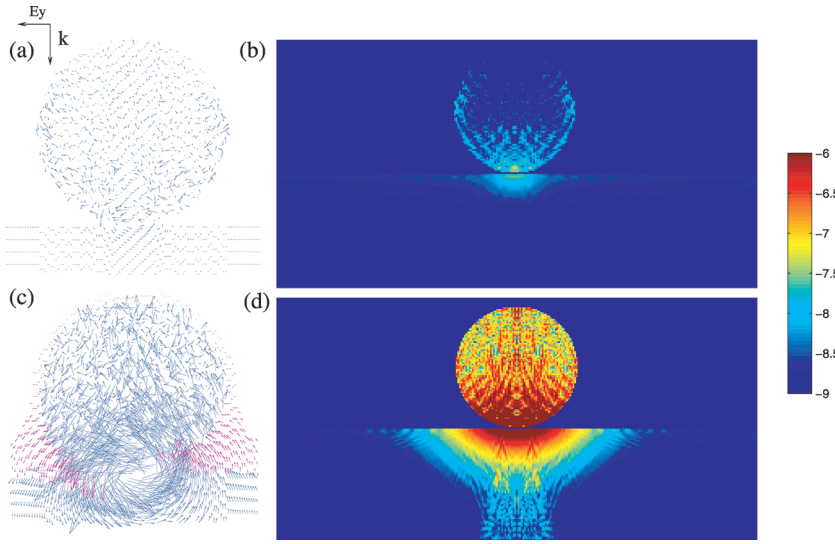

Figure 3. Comparison of the polarization vectors (panels a and c) and of the *local* absorption cross section (panels b and d) for the S0 (upper panels) and S5 (lower panels) excited at the same wavelength ($\lambda_{exc} = 690$ nm). The reported sections are relative to the planes that are dividing the targets in two halves and parallel to the *k* and E_y directions. For graphical reasons, the vectors in panel a were obtained by multiplying the real polarizations ×3, and the 2D color maps of the absorption report values in a 10-base logarithmic scale.

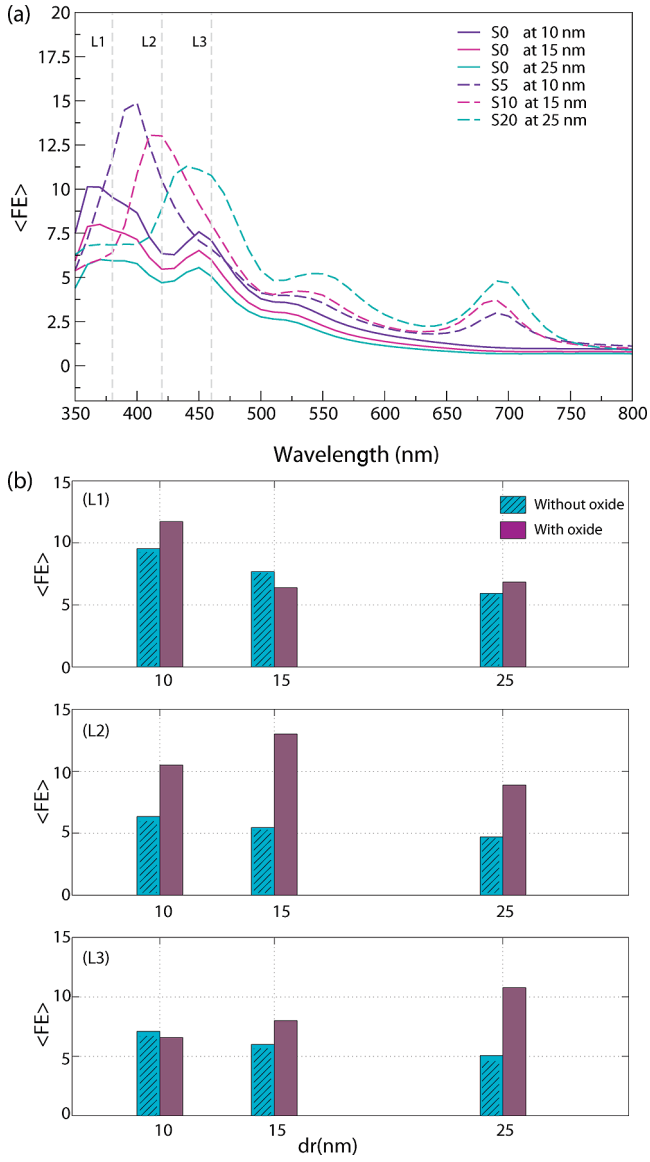

Figure 4. (a) ⟨FE⟩ Trends obtained for the four different thicknesses of the Al_2O_3 layer (0, 5, 10, and 20 nm) in the range 350−800 nm. The three dashed lines concern the S5, S10, and S20 systems with the ⟨FE⟩ computed at a radial distance from structure *d* of 5 nm. The solid lines are related to the ⟨FE⟩ calculated for the S0 system at the same distances. Vertical lines mark different wavelengths on which analysis will be done. (b) Schematization of the results reported in panel a. Histogram L1 is related to λ_{exc} = L1 = 380 nm, histogram L2 is related to λ_{exc} = L2 = 420 nm and histogram (L3) to λ_{exc} = L3 = 460 nm. For each value on the *x*-axes (corresponding to the radial distance from the sphere surface) two bars are reported: the striped-cyan bars concern the system without oxide and the violet ones the system with oxide.

Thus, for λ_{exc} = 690 nm the oxide layer, by redirecting the field as already seen in another recent work,[21] gives origin to a new plasmon resonance effect. The associated optical phenomena of the vortex, which could be due to a phase singularity problem,[53−55] should be taken into account in practical applications of these systems, like nanohole processing/nanofabrication technologies.[52]

We note also that, in contrast to the dipole resonance, the 690 nm-LSPR peak does not shift with the thickness. In fact, for this resonance, the field is almost completely localized near the bottom the sphere. In our model, a thin oxide-layer (5 nm-thick) can already produce a large accumulation of the oxide at the bottom of the sphere and have a significant role in the trapping of radiation (see also Figure S2 in Supporting Information). Additional oxide layers will only cover the region of space above the sphere without influencing the LSPR field distribution and thus without changing the LSPR peak position (Figure 2).

To better assess the role of the oxide spacer for MEF application on the optical behavior of such kind of systems, we investigated also the near-field regime and calculated the electromagnetic effect of the Al_2O_3 layer on the field enhancement.[34] Usually the emitting fluorophores are randomly deposited on top of the oxide layers so that the measured MEF can be ascribed to a global effect of the local field enhancement in the emitters positions. Thus we computed the mean field enhancement by making the average of the FE function on hemispheroidal shells (Ω_d) (see Figure 1) surrounding the target with a radial distance *d* from the sphere surface:

$$\langle FE_d(\lambda_{exc})\rangle = \frac{1}{\Omega_d}\int_{\Omega_d} FE(\lambda_{exc}, \mathbf{r}')d^3\mathbf{r}' \qquad (2)$$

In Figure 4 (panel a) the three dashed lines reproduce the trends of the ⟨FE⟩ for the S5, S10, and S20 systems at a *d* respectively of 10, 15, and 25 nm (corresponding to a fixed distance from the oxide surface of 5 nm). The three solid lines reproduce the trends of the ⟨FE⟩ for the S0 system at the same distances from the Ag surface analyzed for the oxidated system. By going from 10 to 25 nm for the structure without oxide we see a similar profile of the curves, while the height of the curves decreases at increasing *d*, as expected due to increased emitter-metal distances. Three resonances are clearly visible which reproduce those seen in the spectra of Figure 2: the highest at 360 nm which derives by the excitation of the dipolar resonance of the sphere, one at 450 nm which can be attributed to the *E*-enhancement effects due to the limited substrate (see Supporting Information), and a minor one at 690 nm which can be associated to the effect of the oxide on the polarization of the sphere.

The calculations done on the oxidated structures provide a different fundamental result: the presence of an Al_2O_3 layer induces a red-shift of the resonance peaks and a strong enhancement (50%−100%) of the near field for the same exciting wavelength. Considering the main peaks, we have values going from 8.65 to 14.87 for d = 10 nm (λ = 400 nm), from 5.46 to 13.01 for d = 15 nm (λ = 420 nm) and from 5.28 to 11.28 for d = 25 nm (λ = 440 nm). These values probe the active role of an oxide spacer which enlarges the range of the enhancement by transferring the evanescent field without adsorbing it.

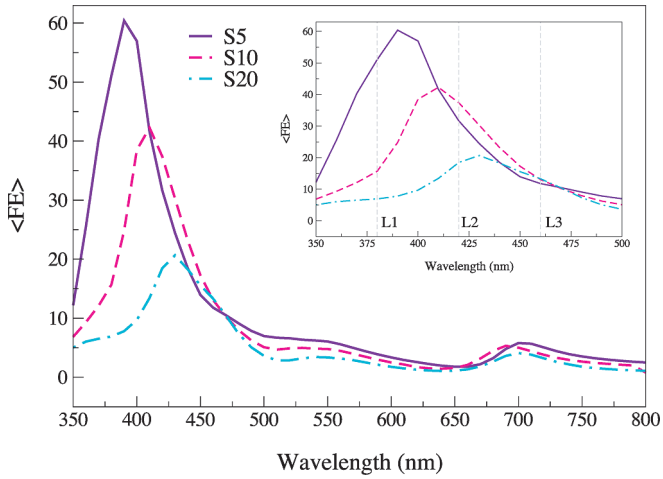

Figure 5. Field enhancement averaged inside 3-nm large medium for different structures, S_n, where *n* indicates the total (oxide + OM) thickness in nanometers. In the inset a zoom of the spectra in the range [350 nm:500 nm] is shown.

In panel b of Figure 4 we report the ⟨FE⟩ as a function of the distance *d*, for three selected wavelengths (L1, L2, and L3). In the case without the oxide the evanescent nature of the near field produces for all the excitation wavelengths a decrease of ⟨FE⟩ at increasing distance from the metal (striped cyan bars in the histograms). Note that we are not considering NR energy transfer, thus the FE is expected to increase at decreasing distance. When an oxide spacer is present, the ⟨FE⟩ has a new, unexpected *nonmonotonic behavior*, and can increase with increasing *d*. This unexpected result should be taken into account in considering the experimental behavior of signals like the fluorescence or the Raman scattering of some emitter located in proximity of a plasmonic nanostructure. Moreover it can explain many open questions about the effects of an oxide spacer. As an example, X. Zhang *et al.*[39] found that the SERS intensity is not decreasing with the Al_2O_3 thickness, and assigned this unusual effect to an increasing number of scattering molecules. The results here presented, suggest another possible explanation: contrary to common belief, the enhancement of the near field can increase with the emitter-substrate distance.

The data reported in Figure 4 consider the near-field enhancements for different oxide layers, measured in the *free space* above the substrate. While direct measurements of the near-field can be obtained, for example using the scanning near-field optical microscopy (SNOM),[56] an indirect measure of the FE is often obtained in actual experiments using emitters (sensing the electromagnetic field) embedded in an organic medium (OM) covering the surface. To verify if the oxide thickness effects on the near field previously discussed are preserved also with an OM covering the system, we performed additional calculations with a 3 nm-OM. We then model the field-enhancement experienced by the emitters in the OM,[57] averaging the computed FE in a shell 3-nm thick (see blue solid arc in Figure 1). In doing this analysis, we replace $\mathbf{E}_{tot}^{syst}(\lambda_{exc}, \mathbf{r})$ in eq 7 (see Methods) by the *excitation field*, that is, the field obtained by considering the difference between the internal field and the self-field (in this case, the field due to the probe-dipole itself).[61]

The results are reported in Figure 5. First of all we can note that the intensities are much larger than those in Figure 4 because the emitter-metal distances are smaller. However the trends between different (oxide + OM) thicknesses are close to those reported previously in Figure 4. For three selected wavelengths (L1, L2, and L3) we found that only for L1 the ⟨FE⟩ is decreasing at increasing oxide thickness. For L2 the same nonmonotonic behavior found in Figure 4b is found, while for L3 the ⟨FE⟩ is almost independent from the oxide thickness.

Thus also in the case where the near-field is measured inside a thin OM, the trend with the oxide layer thickness is preserved. However it is worth noting that a "direct" measurement of the near-field in the empty-space can yield quite different results as compared to an "indirect" one in which an OM is employed. Figure 6 (dashed-line) shows the averaged FE computed (or measured) 5 nm from the Ag sphere surface in the empty space (see inset). The alternative, indirect experiment for the measure of the near-field in which an OM covers the surface (with emitter located again 5 nm from the sphere surface, see inset of Figure 6) will yield completely different results (solid-line). The OM in fact redistributes and increases the near-field intensities. These data attest that an oxide layer, as well as an OM, strongly perturbs the near-field distribution and thus cannot be neglected in experimental measurements.

The previous results can be rationalized considering the near-field distribution induced by the oxide layer. Two-dimensional maps of the FE obtained for the wavelength corresponding to the peaks in Fig-

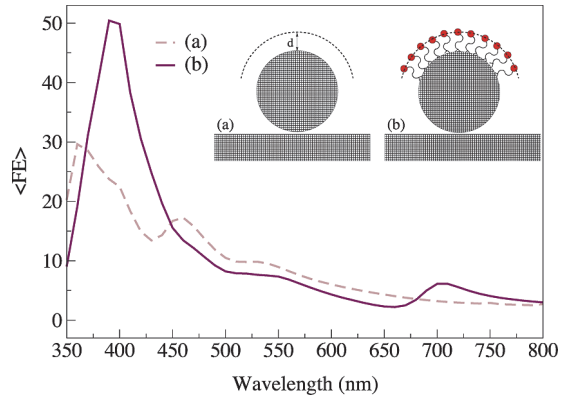

Figure 6. Comparison of the mean field enhancement values obtained at 5 nm for the S0 structure (dashed line) and at 5 nm for the S5 structure (solid line). In the inset a schematization of the two systems is reported.

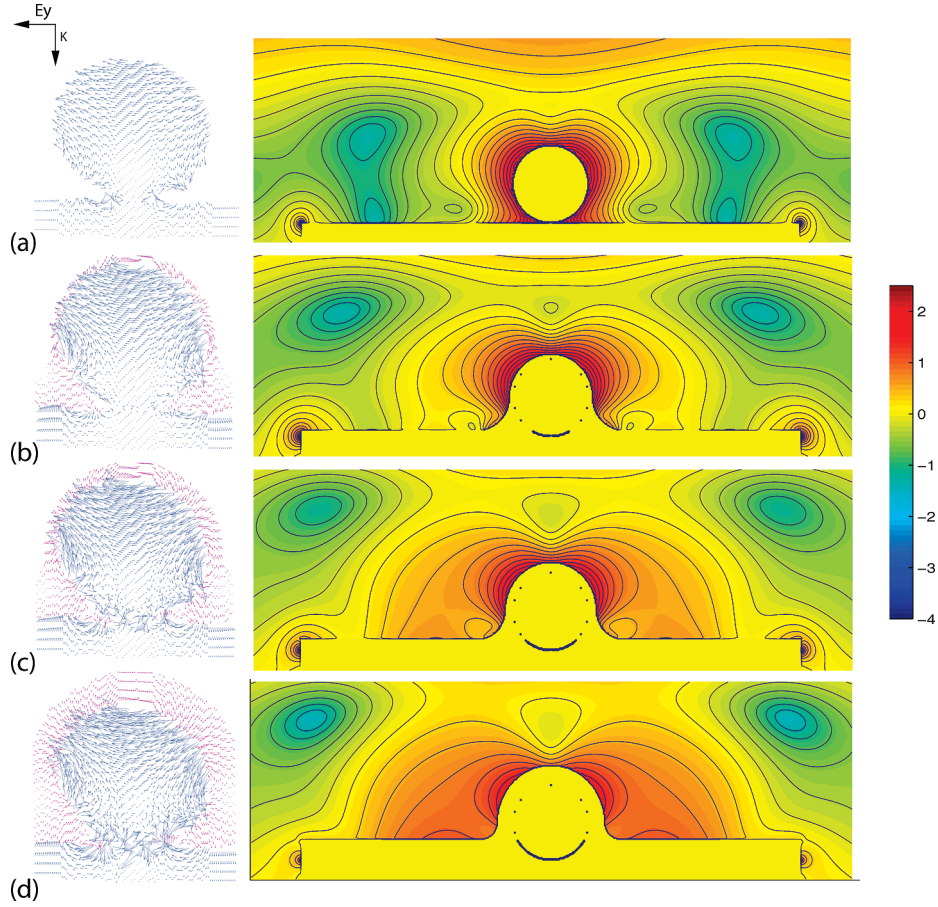

Figure 7. Polarization vectors (real parts) and FE maps obtained at the peaks of Figure 4: at λ_{exc} = 360 nm for S0, at λ_{exc} = 400 nm for S5, at λ_{exc} = 420 nm for S10, and at λ_{exc} = 440 nm for S20. The planes of the plots contain the propagation *x* and the polarization direction *y* and cut the target in two halves. For graphical reasons the illustrated substrate in the polarizations maps corresponds to 20 nm ×100 nm sections, and the scale in the FE maps is a 10 base logarithmic scale.

ure 4 (360, 400, 420, and 440 nm), together with the related polarizations maps, are shown in Figure 7. The preserved bilobe character of the near field around the sphere in the FE maps are related to the dipolar excitation of the Ag sphere, even if the optical response of a metallic nanosphere lying on a substrate with the same dielectric function appears to be very different from that of the particle embedded in an infinite homogeneous background medium.[58] In fact, the presence of the substrate hardly complicates the electromagnetic situation as it breaks the symmetry by introducing the image field. As a consequence the substrate-induced field acting on the entire volume of the NP appears to be no longer homogeneous in space, and multipolar modes of very high order might be excited in addition to the dipolar one. Here these physical effects are strengthened by the oxide presence. The oxide in panels b−d of Figure 7 in fact polarizes itself following the force-lines in the metallic structure and in this way contains the photonic density in the proximity of the metal. The global effect is an important increase of the polarization of the metal. The consequent increased image dipoles induced by the sphere polarization on the substrate move the field on the bottom side of the sphere to the top side of the sphere and spread out of the field in the whole space on the substrate. Thus, in addition to the fundamental contribution of Al_2O_3 in the increase of the near field, the oxide layer also reorganizes the spatial photonic density and changes the angular distribution of the near field as well as that of the far field (details on the angular dependence of the electromagnetic field can be found in the Supporting Information).

CONCLUSIONS

In this work we have shown the oxide-induced effects on the optical behavior of a silver nanosphere touching a silver substrate. Under the action of an external electromagnetic field, the nanoshpere induces a charge distribution on the substrate, which in turn polarizes the MNP. Calculations here reported have attested the importance of an oxide layer in enlarging these interaction effects.

An oxide spacer strongly affects the polarization of a metallic nanostructure by generating a redshift of the extinction spectrum, the appearance of a new absorption resonance, and a strong enhance-

ment of the near field around the nanosphere. With our work we demonstrate in the framework of an electrodynamic theory free by limiting approximations that the near field and then the SERS enhancement do not necessary decay rapidly from the nanoparticle surface, therefore, in the light of this, Al_2O_3 coatings thicker than those commonly used[39] (20 nm instead of 1.0 nm or less) can be considered in SERS applications with the possibility of providing better protection to Ag nanoparticles under a reactive environment.

On the basis of our simulations, the evolution of SPR processing or the design of metal-oxide plasmonic devices can be controlled in a better manner.

METHODS

DDA is one of the most used methods to solve the electromagnetic problem[59] by partitioning a particle into a number *N* of elementary polarizable points called dipoles. The field exciting a dipole is a superposition of the external field and the fields scattered by all other dipoles. This allows one to write a system of *3N* complex linear equations for *N* fields exciting the *N* dipoles

$$\mathbf{E}(\mathbf{r}_j) = \mathbf{E}^{\mathrm{inc}}(\mathbf{r}_j) + \sum_k \mathbf{G}(\mathbf{r}_j - \mathbf{r}_k)\mathbf{P}(\mathbf{r}_k) \tag{3}$$

where the dipoles are given by $\mathbf{P}(\mathbf{r}_k) = \alpha(\mathbf{r}_k)\mathbf{E}(\mathbf{r}_k)$, and $\mathbf{G}(\mathbf{r}_j - \mathbf{r}_k)$ is the free space dyadic Green's function given by the expression[60,61]

$$\mathbf{G}(\mathbf{R}) = \frac{\exp(ikR)}{4\pi R k_B^{\,2}}\left\{k^2\left(\mathbf{1} - \frac{\hat{R}\hat{R}}{R^2}\right) + \frac{ikR - \mathbf{1}}{R^2}\left(\mathbf{1} - 3\frac{\hat{R}\hat{R}}{R^2}\right)\right\} \tag{4}$$

where $\mathbf{R} = \mathbf{r}_j - \mathbf{r}_k$, $R = |\mathbf{R}|$, $\mathbf{1}$ is the identity tensor, and $\hat{R}\hat{R}$ is a tensor with elements $(\hat{R}\hat{R})_{\mu\nu} = R_\mu R_\nu$. Once eq 3 has been solved for the unknown polarizations $\mathbf{P}_j = \mathbf{P}(\mathbf{r}_j)$, the extinction and absorption cross sections C_{ext} and C_{abs} may be evaluated by considering a summation on *N* terms[49]

$$C_{\mathrm{ext}} = \sum_i \sigma_i^{\mathrm{ext}} = 4\pi k \sum_i Im(\mathbf{P}_i \times \mathbf{E}_i^{\mathrm{inc}*}) \tag{5}$$

$$C_{\mathrm{abs}} = \sum_i \sigma_i^{\mathrm{abs}} = 4\pi k \sum_i [Im(\mathbf{P}_i \times \mathbf{E}_i^{\mathrm{exc}*}) - (2/3)k^3|\mathbf{P}_i|^2] \tag{6}$$

where $\mathbf{E}_i^{\mathrm{exc}}$ is the sum of $\mathbf{E}_i^{\mathrm{inc}}$ and the field due to all other dipoles, but excluding the field of the dipole *i* itself. σ_i^{ext} and σ_i^{abs} refer, respectively, to the *local* extinction and absorption cross sections, while Q_{ext} and Q_{abs} are, respectively, the extinction and absorption efficiencies with $Q = C/\pi^*(a_{\mathrm{eff}})^2$ where a_{eff} is the radius of a sphere with the same volume of the entire scatterer. Until now DDA has supported most of the experimental results in plasmonics,[62,63] and it has been applied to a broad range of problems[64−67] (like metal NPs, particle aggregates, rough films, *etc.*) but has not been largely used for particles deposited on an infinite substrate. The difficulty in performing calculations in the last case is purely computational and derives from the necessity to use a box around the particle large enough to simulate the infinite plane or to modify the Green's tensor inside the DDA to take into account the infinite substrate.[68−70] In this case we were able to use a 70 × 500 × 500 dipoles^3 box for the substrate (tests on the dimensions are reported elsewhere[34]) and to perform the entire investigation (spectra, local absorption, polarizations, and near field) in the DDA framework by using high-performance parallel computational facilities. Here to avoid the spurious effects due to the finiteness of the substrate, $\mathbf{E}_{\mathrm{tot}}$ was computed by removing from the field of each complete structure that of the substrate alone according to the formula

$$|\mathbf{E}_{\mathrm{tot}}(\lambda_{\mathrm{exc}}, \mathbf{r})|^2 = |\mathbf{E}_{\mathrm{tot}}^{\mathrm{syst}}(\lambda_{\mathrm{exc}}, \mathbf{r}) - \mathbf{E}_{\mathrm{tot}}^{\mathrm{sub}}(\lambda_{\mathrm{exc}}, \mathbf{r}) + \mathbf{E}_{\mathrm{inc}}(\lambda_{\mathrm{exc}}, \mathbf{r})|^2 \tag{7}$$

assuming $|\mathbf{E}_{\mathrm{inc}}(\lambda_{\mathrm{exc}}, \mathbf{r})|^2 = 1$ and where $\mathbf{E}_{\mathrm{tot}}^{\mathrm{syst}}$ is the total field calculated for the whole structure (sphere plus substrate) and $\mathbf{E}_{\mathrm{tot}}^{\mathrm{sub}}$ is the total field obtained for the isolated finite substrate. To have the exact total field of a nanosphere on an infinite substrate, its reflected field should be added to the calculation,[29] but we can safely assume that its contribution is not significant in making a comparison between different oxide layers. The interdipole distance *d* used for all the calculations was set to 1 nm, a distance small enough to reach convergence for the extinction and absorption sections (error ≤ 0.5% with respect to d = 0.5 nm), as well as for the field values (error ≤ 2%).

We used the DDA implementation proposed by the code of Yurkin and Hoekstra, ADDA,[50] for which calculations are parallelized by dividing the target in multiple slices. This code reads the target geometry by a file of points given in the LF (lab frame) and assigns to each occupied point a polarizability $\alpha_k(\mathbf{r})$. Among the available expressions for the polarizability, LDR (lattice dispersion relation) was used; refractive indexes for Ag were those of Palik.[71]

Acknowledgment. This work was partially founded by the European Research Council (ERC) Starting Grant FP7, Project DEDOM, Grant Agreement No. 207441. We acknowledge the CINECA "Iniziativa Trasverslale Calcolo Parallelo" for allowing us to use the *CLX* and *SP6* resources and M. Margarito for technical support.

Supporting Information Available: Additional results for the extinction spectrum, the absorption spectrum with a silicon dioxide layer, and polar graphs giving informations on the angular distribution of the electromagnetic field. This material is available free of charge *via* the Internet at http://pubs.acs.org.

REFERENCES AND NOTES

1. Wang, H.; Brandt, D. W.; Le, F.; Nordlander, P.; Halas, N. J. Nanorice: A Hybrid Plasmonic Nanostructure. *Nano Lett.* **2006**, *6*, 827–832.
2. Wiley, B. J.; Lipomi, D. J.; Bao, J.; Capasso, F.; Whitesides, G. M. Fabrication of Surface Plasmon Resonators by Nanoskiving Single-Crystalline Gold Microplates. *Nano Lett.* **2008**, *8*, 3023–3028.
3. Novotny, L.; Stranick, S. J. Near-Field Optical Microscopy and Spectroscopy with Pointed Probes. *Annu. Rev. Phys. Chem.* **2006**, *57*, 303–331.
4. Esteban, R.; Vogelgesang, R.; Dorfmuller, J.; Dmitriev, A.; Rockstuhl, C.; Etrich, C.; Kern, K. Direct Near-Field Optical Imaging of Higher Order Plasmonic Resonances. *Nano Lett.* **2008**, *8*, 3155–3159.
5. Prodan, E.; Radloff, C.; Halas, N. J.; Nordlander, P. A Hybridization Model for the Plasmon Response of Complex Nanostructures. *Science* **2003**, *302*, 419–422.
6. Ozbay, E. Plasmonics: Merging Photonics and Electronics at Nanoscale Dimensions. *Science* **2006**, *331*, 189–193.
7. Barnes, W. L.; Dereux, A.; Ebbesen, T. W. Surface Plasmon Subwavelength Optics. *Nature* **2003**, *424*, 824–830.
8. Maier, S. A. In *Plasmonics: Fundamentals and Applications*; Springer: New York, 2007.
9. Mishehenko, M. I.; Travis, L. D.; Lacis, A. A. In *Scattering, Absorption, and Emission of Light by Small Particles*; Cambridge University Press: U.K., 2002.
10. Khlebtsov, N. G.; Trachuk, L. A.; Mel'nikov1, A. G. The Effect of the Size, Shape, and Structure of Metal Nanoparticles

on the Dependence of their Optical Properties on the Refractive Index of a Disperse Medium. *Opt. Spectrosc.* **2005**, *98*, 77–83.
11. Pompa, P. P.; Martiradonna, L.; Della Torre, A.; Della Sala, F.; Manna, L.; De Vittorio, M.; Calabi, F.; Cingolani, R.; Rinaldi, R. Metal-Enhanced Fluorescence of Colloidal Nanocrystals with Nanoscale Control. *Nat. Nanotechnol.* **2006**, *1*, 126–130.
12. Ekgasit, S.; Yu, F.; Knoll, W. Fluorescence Intensity in Surface-Plasmon Field-Enhanced Fluorescence Spectroscopy. *Sens., Actuators B* **2005**, *104*, 294–301.
13. Fleischman, M.; Hendra, P. J.; Mcquillan, A. Raman Spectra of Pyridine Adsorbed at a Silver Electrode. *Chem. Phys. Lett.* **1974**, *26*, 163–166.
14. Jeanmaire, D. J.; Van Duyne, R. P.; Surface Raman Electrochemistry Part, I. Heterocyclic, Aromatic and Aliphatic Amines Adsorbed on the Anodized Silver Electrode. *J. Am. Chem. Soc.* **1977**, *99*, 5215–5217.
15. Albrect, M. G.; Creighton, J. A. Anomalously Intense Raman Spectra of Pyridine at a Silver Electrode. *J. Am. Chem. Soc.* **1977**, *99*, 5215–5217.
16. Chi, Y. S.; Byon, H. R.; Lee, B. S.; Kong, B.; Choi, H. C.; Choi, I. S. Polymeric Rules: Distance-Dependent Emission Behaviours of Fluorophores on Flat Gold Surfaces and Bioassay Platforms Using Plasmonic Fluorescence Enhancement. *Adv. Funct. Mater.* **2008**, *18*, 3395–3402.
17. Stuart, H. R.; Hall, D. G. Enhanced Dipole−Dipole Interaction Between Elementary Radiators Near a Surface. *Phys. Rev. Lett.* **1998**, *25*, 5663–5666.
18. Matveeva, E. G.; Gryczynski, I.; Barnett, A.; Leonenko, Z.; Lakowicz, J. R.; Gryczynski, Z. Metal Particle-Enhanced Fluorescent Immunoassays on Metal Mirrors. *Anal. Biochem.* **2007**, *363*, 239–245.
19. Chu, Y.; Crozier, k. B. Experimental Study of the Interaction between Localized and Propagating Surface Plasmons. *Opt. Lett.* **2009**, *34*, 244–246.
20. Cesario, J.; Gonzalez, M. U.; Cheylan, S.; Barnes, W. L.; Enoch, S; Quidant, R. Coupling Localized and Extended Plasmons to Improve the Light Extraction through Metal Films. *Opt. Express* **2009**, *15*, 10533–10539.
21. Guo, S. H.; Britti, D. G.; Heetderks, J. J.; Kan, H. C.; Phaneuf, R. J. Spacer Layer Effect in Fluorescence Enhancement from Silver Nanowires over a Silver Film; Switching of Optimum Polarization. *Nano Lett.* **2009**, *9*, 2666–2670.
22. Homola, J. In *Surface Plasmon Resonance Based Sensors*; Springer: New York, 2006.
23. Anker, J. N.; Hall, W. P.; Lyandres, O.; Shah, N. C.; Zhao, J.; Van Duyne, R. P. Biosensing with Plasmonic Nanosensors. *Nat. Mater.* **2008**, *7*, 442–453.
24. Stewart, M.; Anderton, C; Thompson, L.; Maria, J.; Gray, S.; Rogers, J.; Nuzzo, R. Nanostructured Plasmonic Sensor. *Chem. Rev.* **2008**, *108*, 494–521.
25. Lal, S.; Grady, N. K.; Kundu, J.; Levin, C. S; Lassiter, J. B.; Halas, N. J. Tailoring Plasmonic Substrates for Surface Enhanced Spectroscopies. *Chem. Soc. Rev.* **2008**, *37*, 898–911.
26. Westphalen, M.; Kreibig, U.; Rostalski, J.; Luth, H.; Meissner, D. Sol. Metal Cluster Enhanced Organic Solar Cells. *Energy Mater. Sol. Cells* **2000**, *61*, 97–105.
27. Oulton, R. F.; Sorger, V. J.; Zentgraf, T.; Ma, R. M.; Gladde, C.; Dai, L.; Bartal, G.; Zhang, X. Plasmon Lasers at Deep Subwavelength Scale. *Nature* **2009**, *461*, 629–632.
28. Bhowmick, S.; Saini, S.; Shenoy, V. B.; Bagchi, B. Resonance Energy Transfer from a Fluorescent Dye to a Metal Nanoparticle. *J. Chem. Phys.* **2006**, *125*, 181102–6.
29. D'Agostino, S.; Pompa, P. P.; Chiuri, R.; Phaneuf, R. J.; Britti, D. G.; Rinaldi, R.; Cingolani, R.; Della Sala, F. Enhanced Fluorescence by Metal Nanospheres on Metal Substrates. *Opt. Lett.* **2009**, *34*, 2381–2383.
30. Akimov, Y. A.; Ostrikov, K.; Li, E. P. Fluorescence Intensity in Surface-Plasmon Field-Enhanced Fluorescence Spectroscopy. *Plasmonics* **2009**, *4*, 107–113.
31. Aouani, H.; Wenger, J.; Gerard, D.; Rigneault, H.; Devaux, E.; Ebbesen, T. W.; Mahdavi, F.; Xu, T.; Blair, S. Crucial Role of the Adhesion Layer on the Plasmonic Fluorescence Enhancement. *ACS Nano* **2009**, *3*, 2043–2048.
32. Whitney, A. V.; Elam, J. W.; Stair, P. C.; Van Duyne, R. P. Toward a Thermally Robust Operando Surface-Enhanced Raman Spectroscopy Substrate. *J. Phys. Chem. C* **2007**, *111*, 16827–16832.
33. Sung, J.; Kosuda, K. M.; Zhao, J.; Elam, J. W.; Spears, K. G.; Van Duyne, R. P. Stability of Silver Nanoparticles Fabricated by Nanosphere Lithography and Atomic Layer Deposition to Femtosecond Laser Excitation. *J. Phys. Chem. C* **2008**, *112*, 5707–5714.
34. D'Agostino, S.; Della Sala, F. Electromagnetic Modelling of the Optical Behaviour of Silver Nanospheres on Dielectric Substrates: The Role of a Silver Buffer Layer. *Superlattices Microstruct.* **2010**, *47*, 55–59.
35. Jensen, T. R.; Malinsky, M. D.; Haynes, C. L.; Van Duyne, R. P. Nanosphere Lithography: Tunable Localized Surface Plasmon Resonance Spectra of Silver Nanoparticles. *J. Phys. Chem. B* **2000**, *104*, 10549–10556.
36. Zhang, X.; Hicks, E. M.; Zhao, J.; Schatz, G. C.; Van Duyne, R. P. Electrochemical Tuning of Silver Nanoparticles Fabricated by Nanosphere Lithography. *Nano Lett.* **2005**, *5*, 1503–1507.
37. Whitney, A. V.; Elam, J. W.; Zou, S.; Zinovev, A. V.; Stair, P. C.; Schatz, G. C.; Van Duyne, R. P. Localized Surface Plasmon Resonance Nanosensor: A High-Resolution Distance-Dependence Study Using Atomic Layer Deposition. *J. Phys. Chem. B* **2005**, *109*, 20522–20528.
38. Zhang, X.; Whitney, A. V.; Zhao, J.; Hicks, E. M.; Van Duyne, R. P. Advances in Contemporary Nanosphere Lithographic Techniques. *J. Nanosci. Nanotechnol.* **2006**, *6*, 1920–1934.
39. Zhang, X.; Zhao, J.; Whitney, A. V.; Elam, J. W.; Van Duyne, R. P. Ultrastable Substrates for Surface-Enhanced Raman Spectroscopy: Al_2O_3 Overlayers Fabricated by Atomic Layer Deposition Yield Improved Anthrax Biomarker Detection. *J. Am. Chem. Soc.* **2006**, *128*, 10304–10309.
40. Chan, G. H.; Zhao, J.; Hicks, E. M.; Schatz, G. C.; Van Duyne, R.P. Plasmonic Properties of Copper Nanoparticles Fabricated by Nanosphere Lithography. *Nano Lett.* **2007**, *7*, 1947–1952.
41. Worthing, P. T.; Amos, R. M.; Barnes, W. L. Modification of the Spontaneous Emission Rate of Eu^{3+} Ions Embedded within a Dielectric Layer above a Silver Mirror. *Phys. Rev. A* **1999**, *59*, 865–872.
42. Murray, W. A.; Suckling, J. R.; Barnes, W. L. Overlayers on Silver Nanotriangles: Field Confinement and Spectral Position of Localized Surface Plasmon Resonances. *Nano Lett.* **2006**, *6*, 1772–1777.
43. Rindzevicius, T.; Alaverdyan, Y.; Käll, M.; Murray, W. A.; Barnes, W. L. Long-Range Refractive Index Sensing Using Plasmonic Nanostructures. *J. Phys. Chem. C* **2007**, *111*, 11806–11810.
44. Malinsky, M. D.; Kelly, K. L.; Schatz, G. C.; Van Duyne, R. P. Nanosphere Lithography: Effect of Substrate on the Localized Surface Plasmon Resonance Spectrum of Silver Nanoparticles. *J. Phys. Chem. B* **2001**, *105*, 2343–2350.
45. Yamaguchi, T.; Yoshida, S.; Kinbara, A. Optical Effect of the Substrate on the Anomalous Absorption of Aggregated Silver Films. *Thin Solid Films* **1974**, *21*, 173–187.
46. Ruppin, R. Surface Modes and Optical Absorption of a Small Sphere above a Substrate. *Surf. Sci.* **1983**, *127*, 108–118.
47. Gozhenko, V. V.; Grechko; L, G.; Whites, K. W. Electrodynamics of Spatial Clusters of Spheres: Substrate Effects. *Phys. Rev. B.* **2003**, *68*, 125422-1–125422-16.
48. Chan, G. H.; Zhao, J.; Hicks, E. M.; Schatz, G. C.; Van Duyne, R. P. Plasmonic Properties of Copper Nanoparticles Fabricated by Nanosphere Lithography. *Nano Lett.* **2007**, *7*, 1947–1952.
49. Draine, B. T.; Flatau, P. J. Discrete-Dipole Approximation for Scattering Calculations. *J. Opt. Soc. Am. A* **1994**, *11*, 1491–1499.
50. Yurkin, M. A.; Hoekstra, A. G. *ADDA*; http://code.google.com/p/a-dda/.

51. D'Agostino, S. Della Sala, F. Routine for the Near Field at http://code.google.com/p/a-dda/downloads/detail?name=near_field_1_01.tar.gz&can=2&q=.
52. Tanaka, Y.; Nedyalkov, N. N.; Obara, M. Enhanced Near-Field Distribution inside Substrates Mediated with Gold Particle: Optical Vortex and Bifurcation. *Appl. Phys. A* **2009**, *97*, 91–98.
53. Wang, Z. B.; Luk'yanchuk, B. S.; Hong, M. H.; Lin, Y.; Chong, T. C. Energy Flows around a Small Particle Investigated by Classical Mie Theory. *Phys. Rev. B* **2004**, *70*, 035418-1–035418-12.
54. Tribelsky, M. I.; Luk'yanchuk, B. S. Anomalous Light Scattering by Small Particles. *Phys. Rev. Lett.* **2006**, *97*, 263901-1–263902-4.
55. Luk'yanchuk, B. S.; Ternovsky, V. Light scattering by a Thin Wire with a Surface-Plasmon Resonance: Bifurcations of the Poynting Vector Field. *Phys. Rev. B.* **2006**, *73*, 235432-1–235432-12.
56. Yasushi Oshikane, Y.; Kataoka, T.; Okuda, M.; Hara, S.; Inoue, H.; Nakano, M. Observation of Nanostructure by Scanning Near-Field Optical Microscope with Small Sphere Probe. *Sci. Technol. Adv. Mater.* **2007**, *8*, 181–185.
57. Typical organic material has a refractive index in the range (1.7−1.8), very close to the one of Al_2O_3. For simplicity to the model the organic medium we use the refractive index of the latter.
58. Noguez, C. Optical Properties of Isolated and Supported Metal Nanoparticles. *Opt. Mater.* **2005**, *27*, 1204–1211.
59. Comberg, U.; Wriedt, T. Comparison of Scattering Calculations for Aggregated Particles Based on Different Models. *J. Quant. Spectrosc. Radiat. Transfer* **1999**, *63*, 149–162.
60. Martin, O. J. F.; Piller, N. B. Electromagnetic Scattering in Polarizable Backgrounds. *Phys. Rev. E* **1998**, *58*, 3909–3915.
61. Yurkin, M. A.; Hoekstra, A. G. The Discrete Dipole Approximation: An Overview and Recent Developments. *J. Quant. Spectrosc. Radiat. Transfer* **2007**, *106*, 558–589.
62. Yang, P.; Portales, H.; Pileni, M. P. Identification of Multipolar Surface Plasmon Resonances in Triangular Silver Nanoprisms with Very High Aspect Ratios Using the DDA Method. *J. Phys. Chem. C* **2009**, *113*, 11597–11604.
63. Rang, M.; Jones, A. C.; Zhou, F.; Li, Zhi-Y.; Wiley, B. J.; Xia, Y.; Raschke, M. B. Optical Near-Field Mapping of Plasmonic Nanoprisms. *Nano Lett.* **2008**, *8*, 3358–3363.
64. Yang, W. H.; Schatz, G. C.; Van Duyne, R. P. Discrete Dipole Approximation for Calculating Absorption and Raman Intensities for Small Particles with Arbitrary Shapes. *J. Chem. Phys.* **1995**, *103*, 869–875.
65. Kelly, K. L.; Coronado, E.; Zhao, L. L.; Schatz, G. C. The Optical Properties of Metal Nanoparticles: The Influence of Size, Shape, and Dielectric Environment. *J. Phys. Chem. B* **2003**, *107*, 668–677.
66. Hao, E.; Schatz, G. C. Electromagnetic Fields around Silver Nanoparticles and Dimers. *J. Chem. Phys.* **2004**, *120*, 357–366.
67. Kelly, K. L.; Lazarides, A. A.; Schatz, G. C. Computational Electromagnetics of Metal Nanoparticles and Their Aggregates. *Nanotechnology* **2001**, *3*, 67–73.
68. Schmehl, R.; Nebeker, B. M.; Hirleman, E. D. Discrete-Dipole Approximation for Scattering by Features on Surfaces by means of a Two-Dimensional Fast Fourier Transform Technique. *J. Opt. Soc. Am. A* **1997**, *14*, 3026–3036.
69. Bae, E.; Zhang, H.; Hirleman, E. D. Application of the Discrete Dipole Approximation for Dipoles Embedded in Film. *J. Opt. Soc. Am. A* **2008**, *25*, 1728–1736.
70. Martin, O. J. F. Efficient Scattering Calculations in Complex Backgrounds. *Int. J. Electron. Commun.* **2004**, *58*, 93–99.
71. Palik, E. D. *Handbook of Optical Constants of Solids*; Academic Press: New York, 1985.